RSC Advances

ROYAL SOCIETY OF CHEMISTRY

www.rsc.org/advances

$(K_{0.5}Na_{0.5})NbO_3:Eu^{3+}/Bi^{3+}$: a novel highly efficient, red light-emitting material with superior water resistance behavior

Qiwei Zhang[1], Haiqin Sun [1*], Tao Kuang[1], Ruiguang Xing[1], Xihong Hao[1*]

[1] School of Materials and Metallurgy, Inner Mongolia University of Science and Technology, 7# Arerding Street, Kun District, Baotou 014010, China

Abstract

Materials emitting red light (~ 611 nm) under excitation with blue light (440 ~ 470 nm) are highly desired for fabricating high-performance white light-emitting diodes (LEDs). Conventionally used red light-emitting materials (e.g., $Y_2O_3:Eu^{3+}$ or $Y_2O_2S:Eu^{3+}$) exhibit a relatively poor blue light-absorption and a weak chemical stability. In this paper, we reported on a novel red light-emitting material based on a $(K_{0.5}Na_{0.5})NbO_3$ (KNN) matrix co-doped with Bi^{3+} and Eu^{3+} showing a strong absorption in the blue light region and superior water resistance properties. The crystal structure, photoluminescence, thermal stability, energy transfer mechanism and water resistance behavior of the samples were systematically investigated. A strongly enhanced red light-emission at 616 nm originating from the $^5D_0 \rightarrow {}^7F_2$ transition of Eu^{3+} ions was observed after adding Bi^{3+} ions as an alternative to increasing the Eu^{3+} concentration due to the energy transfer from Bi^{3+} to Eu^{3+}. After adding 0.05 mol of Bi^{3+} as sensitizer, the sample with the composition of $(K_{0.5}Na_{0.5})_{0.90}Eu_{0.05}Bi_{0.05}NbO_3$ exhibited the strongest red light-emission and a high quantum yield under 465 nm excitation. Doping with Bi^{3+} also endowed the KNN:Eu^{3+} samples with a good thermal stability (83% of the initial intensity at 150 °C) and a superior water resistance

[1*] Corresponding author: Tel.: +86 472 6896872; Fax: +86 472 5951571
E-mail: a8082sz@imust.edu.cn (H. Sun), xhhao@imust.edu.cn (X. Hao)

behavior(94.3% of the initial intensity after 40 h of immersion). These results demonstrate the great potential of the Bi^{3+}/Eu^{3+} co-doped KNN material for a future application in white LEDs and novel multifunctional devices.

***Keywords*:** Lead-free ceramics; Photoluminescence; Water resistance

1. Introduction

Lead-free piezoelectric materials, such as $BaTiO_3$ (BT), $(K_{0.5}Na_{0.5})NbO_3$ (KNN), $(Bi_{0.5}Na_{0.5})TiO_3$) (BNT), and their derivatives, have stimulated an increasing practical interest due to their excellent ferroelectric/piezoelectric properties and are widely used in smart sensors, actuators, piezoelectric transducers, and other electronic devices.[1-4] Among these lead-free piezoelectric materials, sodium potassium niobate (KNN), i.e., a solid solution of ferroelectric $KNbO_3$ and anti-ferroelectric $NaNbO_3$ in the ratio of 1:1 with an $A^{1+}B^{5+}O_3^{2+}$ perovskite structure, is currently one of the most widely exploited materials due to its low coercive electric fields, high depolarization temperatures, and excellent piezoelectric properties (d_{33} of up to 80 pC N^{-1}, T_c~420 °C, Pr~33 μC cm^{-2}).[5] The piezoelectric properties of KNN-based materials can be significantly enhanced by optimizing the processing conditions and by ion substitution (A-site and/or B-site substitution).[6] For example, the piezoelectric constant d_{33} can reach up to 416 pC N^{-1} in Li, Ta, and Sb-doped KNN ceramics, which is comparable to values obtained for $Pb(Zr,Ti)O_3$.[7] Therefore, the majority of studies on KNN-based ceramics focus on an enhancement of the piezoelectric properties and a practical application in micro-electronic devices.

In addition to applications utilizing the piezoelectric and ferroelectric properties of KNN-based materials, e.g. in piezoelectric transducers, KNN is currently considered as a promising host matrix for luminescent materials, due to their superior chemical stability, successive structural phase transitions and non-linear optical behavior, with the luminescence achieved through the introduction of rare earth (RE) ions.[8-10] In our previous work, we have shown that the emission of red light (617 nm and 650 nm) and green light (528 nm) can be realized in Pr^{3+}-doped KNN materials.[11] In fact, RE elements not only act as activator ions to achieve luminescence, but also act as structural

modifiers, thereby improving the electrical properties of some ferroelectric perovskite-type compounds.

Recently, several studies on RE-doped ferroelectric oxides have been published.[12-16] The simultaneous existence of luminescence and ferroelectric/piezoelectric properties has been realized, as well as a dual-enhancement of both the ferro-/piezoelectric and the photoluminescence performance in Pr^{3+}-doped KNN ceramics.[17] These results indicate that RE-doped ferroelectric oxides may see a potential application in novel multifunctional devices by integrating at least two characteristics. Unfortunately, compared to traditional phosphors, such as alkaline earth sulfide/oxysulfide phosphors and nitrides/oxynitrides, RE-doped ferroelectric oxides exhibit a relatively low luminescence efficiency (quantum yield < 15%), due to their relatively large phonon energy.[18-20] Some approaches on controlling the electric fields and increasing the RE-doping concentrations were recently proposed by Hao *et al.*[14] and Liu *et al.*[21] However, so far, only a few studies have been reported on high-efficient RE-doped ferroelectric/piezoelectric materials. Hence, it is urgent to further improve the luminescence efficiency of this kind of materials to values comparable to traditional phosphors.

Eu^{3+} ions have been widely used in most commercial phosphors as activators, showing red light-emission at about 613 nm.[22,24] Furthermore, the red light-emission intensity can be remarkably improved by an energy transfer from sensitizer ions to RE ions. Sensitizers can effectively compensate for the low luminescence efficiency of RE ions resulting from the small absorption cross section of the parity-forbidden intra-4f transition.[25,26] Among the potential sensitizers, Bi^{3+} ions have been shown to be a very good sensitizer for Eu^{3+} ions. For example, Datta *et al.* reported an increase in the emission intensity by a factor of 2 for Bi^{3+}-doped YVO_4:Eu materials.[27] Recently,

Liu *et al.* reported on the ZnB_2O_4:10%Eu:10%Bi system.[21] The emission intensity and quantum efficiency of the phosphor could be increased by 14% and 6%, respectively, due to the introduction of Bi^{3+} ions. These results suggest that it is possible to design and fabricate highly efficient red light-emitting ferroelectric/piezoelectric materials.

In this work, a novel lead-free luminescent ferroelectric material has been fabricated by co-doping Bi^{3+} and Eu^{3+} ions into a $(K_{0.5}Na_{0.5})TiO_3$ (KNN) host material. To the best of our knowledge, the photoluminescent properties of Bi^{3+}/Eu^{3+}-co-activated KNN ceramics have not been investigated so far. It is expected that a highly efficient red light-emission with a quantum yield of ~ 0.34 can be achieved through an energy transfer from the sensitizer Bi^{3+} to the activator Eu^{3+} in the KNN host as an alternative to increasing the Eu^{3+} ion concentration, which might allow for an enhancement of luminescence efficiency at much lower cost. In this study, we systematically investigated the effect of the Bi^{3+} ions on the processing, phase structure, photoluminescence, thermal stability and water resistance properties of Bi^{3+}/Eu^{3+}-doped KNN ceramics.

2. Material and methods

2.1. Sample preparation

The KNN samples co-doped with Bi^{3+} and Eu^{3+} were synthesized utilizing the conventional solid-state reaction method. K_2CO_3 (99%, Alfa Aesar), Na_2CO_3 (99.5%, Alfa Aesar), Nb_2O_5 (99.5%, Alfa Aesar), Eu_2O_3 (99.99%, Alfa Aesar) and Bi_2O_3 (99.975%, Alfa Aesar) powders were used as raw materials and weighted according to the formula: $(K_{0.5}Na_{0.5})_{0.95-x}Eu_{0.05}Bi_xNbO_3$ (abbreviated as $KNEB_xN$, x = 0, 0.005, 0.015, 0.025, 0.04, 0.05, 0.07, 0.10, 0.15). These weighted powders were mixed with ethanol, dried at 100 °C, and calcined in an alumina crucible at 880 °C for 6 h in air. Then, the calcined powders were crushed and mixed again. The obtained powders were mixed and

pulverized with an 8 wt% polyvinyl alcohol binder and pressed into disk-shaped pellets with a diameter of 10 mm and a thickness of 1 mm thickness at a pressure of 100 MPa. Then, to remove the binder, the pellets were annealed at 550 °C for 10 h using a heating rate of 1 °C min^{-1}.

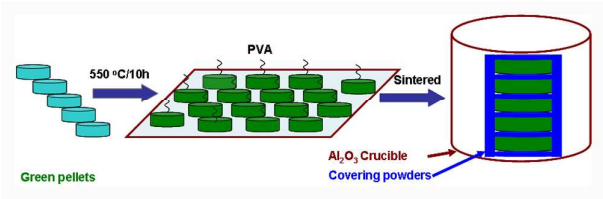

Fig. 1 Schematic of the sintering process of the $KNEB_xN$ ceramics.

In order to suppress the evaporation of alkali elements during the sintering process, the green pellets with different composition were covered with the corresponding powders, and sintered at 1130-1150 °C for 4 h in air. The sintering process is schematically illustrated in Fig. 1. To investigate the effect of the sintering temperature on the luminescence properties, the sample with x = 0.05 was sintered at 900, 1000, 1050, 1080, 1110, 1130, 1150, 1170, and 1190 °C for 4 h in air, respectively.

2.2. Characterization

X-ray diffraction (XRD) analysis was performed to identify the phase structure of the samples utilizing Cu Kα radiation (D8 Advanced, Bruker, Germany). The microstructure of the sintered samples was investigated by field emission scanning electron microscopy (FE-SEM, JSM EMP-800, JEOL, Japan). Inductively coupled plasma atomic emission spectroscopy (ICP-AES) (PROFILE SPEC, Leeman, AMERICA) was adopted to investigate the degree of volatilization of K/Na/Bi at high temperature.

The photoluminescence (PL) and photoluminescence excitation (PLE) spectra were recorded on a spectrofluorometer (F-7000, HITACHI, Japan) equipped with a temperature-controlled chamber

(Linkam, THMS600, United Kingdom) in the temperature range from 20 to 320 °C and the wavelength range from 200 nm to 750 nm, with a 0.2 nm step size, at a scan speed of 240 nm min^{-1}, a PMT voltage of 700 V, a response time of 0.002 s, and excitation and emission slits of 2.5 nm and 5.0 nm, respectively. The diffuse reflectance spectra of the samples were measured using a UV/Vis spectrophotometer (U-3900, HITACHI, Japan).

Before recording the PL and PLE spectra, all samples were polished to a thickness of 0.5 mm and washed with ethanol. The quantum yield and decay curves of the samples were measured using a combined steady state & time resolved fluorescence spectrometer (FLS920, Edinburgh Instruments, United Kingdom). To measure the materials' resistance to water, the powder samples were immersed in distilled water for 0, 1 h, 5 h, 10 h, 20 h and 40 h, respectively. Afterwards, the powders were dried at 100 °C prior to the PL measurements.

3. Results and discussions

3.1. Microstructure and crystal structure

A representative SEM image of the $KNEB_xN$ ($x = 0.05$) sample sintered at 1150 °C is shown in Fig. 2(a). The sample exhibits a well-faceted and uniform morphology. A similar morphology was observed for the other samples (not shown here). The crystal structure of KNN at room temperature is an orthorhombic phase with Amm2 symmetry, and the perovskite-type ABO_3 subcell exhibits a monoclinic symmetry with the lattice parameters $a_m = c_m > b_m$, as illustrated in Fig. 2(b).

The XRD patterns (2θ range from 20 to 80°) obtained for the $KNEB_xN$ ceramic samples with different Bi^{3+} concentrations sintered at 1130-1150 °C are shown in Fig. 2(c). The samples with $x \leq 0.07$ exhibit a main phase of KNN with a perovskite-type ABO_3 structure and a small amount of a second phase, which was identified as the $EuNbO_4$ phase, as reported by Fang *et al.*[28] The samples

with a comparatively higher Bi^{3+} concentration (x>0.07) show additional diffraction lines, which could be attributed to the $BiNbO_4$ phase.[29] Because of the weak intensity of these impurity phase peaks, the influence of the impurity phase on the photoluminescence of $KNEB_xN$ is neglected in this paper.

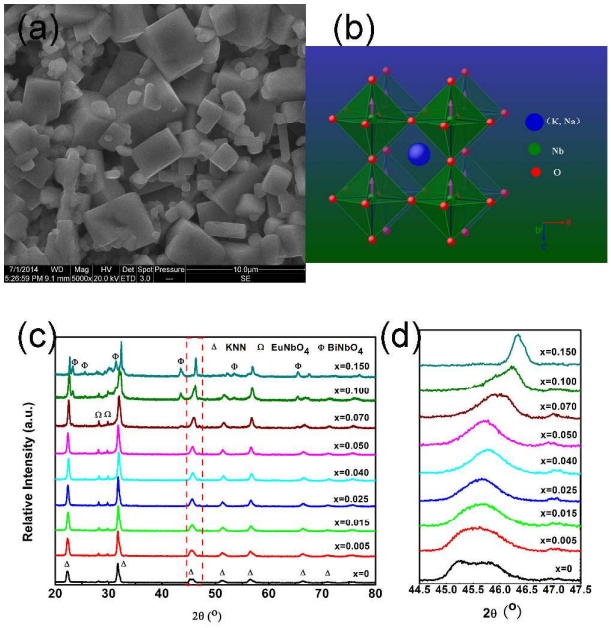

Fig. 2 (a) SEM image of the selected $KNEB_xN$ (x=0.05) sample. (b) The perovskite type ABO_3 subcell of KNN. (c) XRD patterns of $KNEB_xN$ ceramics (x=0, 0.005, 0.045, 0.025, 0.040, 0.050,0.070, 0.100, 0.150). (d) The diffraction peaks from 44.5° to 47.5°.

These results suggest that the solubility limit of Bi^{3+} ions in the KNN: Eu matrix is about 0.07 mol. According to Fig. 2(d), the diffraction peaks of the (200) plane at 2θ= 45° gradually shift to higher angles with increasing Bi^{3+} content due to the relatively smaller ionic radius of K^+ [1.64 Å, CN=12] compared to Bi^{3+} [1.45 Å, CN=12], resulting in a shrinkage of the KNN cell volumes. Based on the ionic radius and the ions' charges, we believe that Eu^{3+} and Bi^{3+} tend to occupy the A sites. In addition, a gradual broadening of the diffraction peaks was observed if the Bi^{3+} content exceeded 0.07 mol. This could be caused by the generation of A vacancies (V_A): $3\ K^+ \rightarrow Bi^{3+} + V_K$.

Similar results were observed for $CaMoO_4$ co-doped with Bi^{3+} and Eu^{3+}.[30]

It is known that the volatility of alkali elements in KNN-based ceramics by normal sintering is generally unavoidable, then resulting in composition deviation from the starting one.[31] In this paper, considering the volatility of K/Na/Bi, we adopted the inductively coupled plasma atomic emission spectroscopy (ICP-AES) to investigate their loss degree and stoichiometric fluctuation behaviors. The measured results are shown in Fig. 3. It can be clearly seen that the volatilization of Na is the most serious, compared to the the volatilization of K and Bi elements. The degree of volatilization of Bi and K elements changes slightly with increasing Bi concentrations. The K/Na mole ratio as a function of Bi concentrations is shown in the inset of Fig. 3. The apparent deviation from 1 in K/Na ratio indicates clearly that the Na elements volatilize more seriously than the K elements.[32]

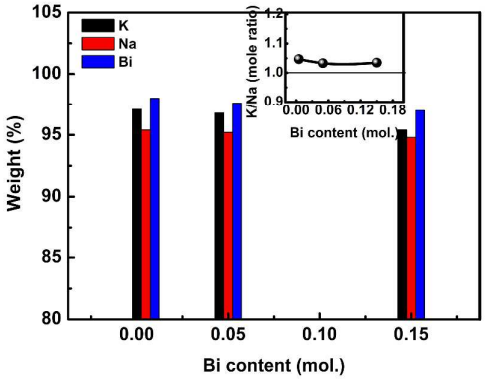

Fig. 3 The degree of volatilization of K, Na and Bi elements in $KNEB_xN$ ceramics (x=0.005, 0.050, 0.150), the inset is K/Na mole ration as a function of Bi concentrations.

3.2 Luminescence properties and energy transfer mechanism

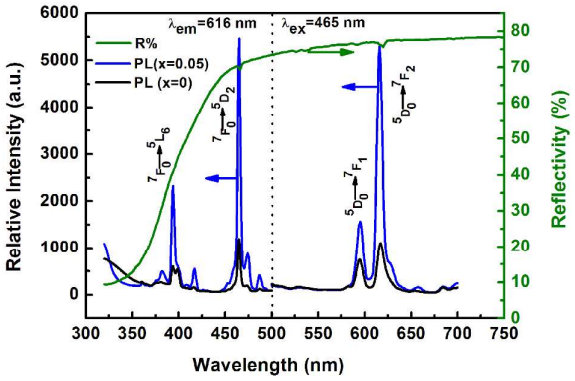

Fig. 4 Room temperature PLE, PL and diffuse reflectance spectra of the $KNEB_xN$ (x=0, 0.05) sample.

The typical photoluminescence (PL) and excitation (PLE) spectra obtained for the $KNEB_xN$ (x = 0, 0.05) samples at room temperature are shown in Fig. 4. The PL and PLE spectra of the samples with and without Bi^{3+} doping show a similar shape and no shift of excitation or emission peaks, indicating that the introduction of Bi^{3+} has no effect on the PL and PLE patterns. However, Bi^{3+} greatly enhances their relative intensity. In Fig. 4 (left image), the PLE spectra recoded at 616 nm exhibit two strong sharp absorptions located at 394 nm and 465 nm, respectively. These excitation peaks are attributed to the typical f-f transition of Eu^{3+}, resulting from an excitation from the $^7F_0$ ground state to the $^5L_6$ and $^5D_2$ excited states, respectively, corresponding to the $^7F_0 \rightarrow {}^5L_6$ (394 nm) and $^7F_0 \rightarrow {}^5D_2$ (465 nm) transition. The strongest absorption appears in the blue light region (465 nm), whose band covers the emission wavelength of all commercial blue LED chips (420-470 nm), emphasizing the material's potential for an application in white light-emitting diodes (W-LEDs).[33]

The emission spectra excited by 465 nm light shows a strong line emission peak centered at 616 nm and a weak line emission peak at 595 nm, as shown in Fig. 4 (right). These two line emissions

are ascribed to the 4f-4f transitions of Eu^{3+}, i.e., $^5D_0 \rightarrow {}^7F_1$ (595 nm) and $^5D_0 \rightarrow {}^7F_2$ (616 nm). Compared to the emission intensity at 595 nm, the $^5D_0 \rightarrow {}^7F_2$ transition at 616 nm exhibits a stronger red light-emission intensity with a full width at half maximum (FWHM) of 6 nm. Furthermore, the positions of the PLE and PL peaks observed above are in good agreement with the diffuse reflectance spectrum of the $KNEB_xN$ (x = 0.05) sample, as shown in Fig 4. In the reflectance spectrum, two absorption bands with maxima at ~466 nm and ~617 nm were observed. The high-energy band corresponds to the absorption of the KNN host lattice, whereas the low-energy absorption band is attributed to the characteristic f-f transitions of Eu^{3+}.

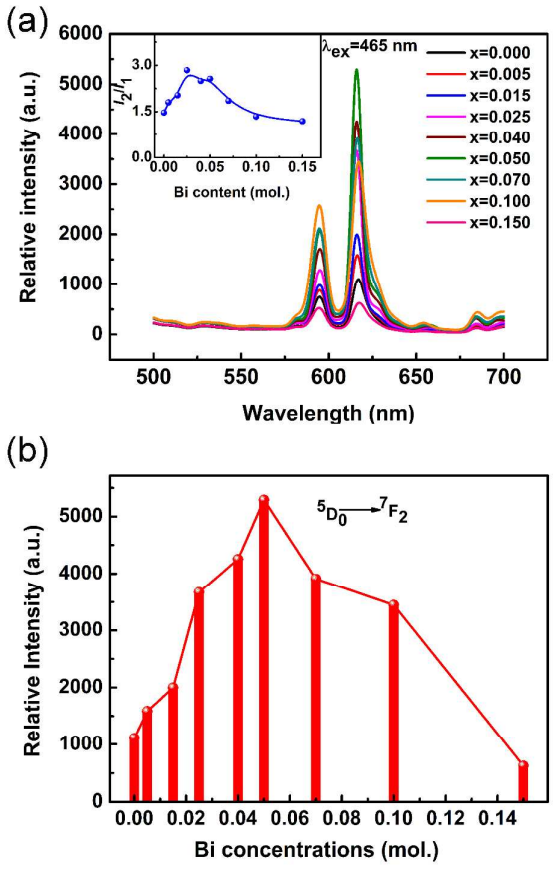

Fig. 5 (a) PL spectra of the $KNEB_xN$ ceramics (x=0, 0.005, 0.045, 0.025, 0.040, 0.050,0.070, 0.100, 0.150) excited by 465 nm at room temperature, the inset is the intensity ratio of

I_2/I_1 on Bi^{3+} concentrations. (b) The dependence of the emission intensity ($^5D_0 \rightarrow {}^7F_2$) on Bi^{3+} concentrations.

The PL spectra of $KNEB_xN$ samples with different Bi^{3+} content (x = 0, 0.005, 0.015, 0.025, 0.04, 0.05, 0.07, 0.10, 0.15) recorded under 465 nm blue light excitation are shown in Fig. 5. Similar to the results presented in Fig. 4, the emission spectra of all samples shows two line emission bands at 595 nm and 616 nm, assigned to the intra-4f transition from the excited $^5D_0$ state to the ^7F_J (J=1,2) ground state of Eu^{3+}. The shape and position of the emission peaks do not change when the Bi^{3+} content is varied, whereas the emission intensity shows a strong dependence on the Bi^{3+} doping concentration.

According to the Judd-Ofelt theory, the $^5D_0 \rightarrow {}^7F_1$ transition is a magnetic-dipole transition, which is nearly insensitive to local crystal field variations, while the forced electric dipole (ED) transition at 616 nm ($^5D_0 \rightarrow {}^7F_2$) is sensitive to the local environment.[34] Therefore, the intensity ratio R (R = I_2/I_1) of the $^5D_0 \rightarrow {}^7F_2$ (I_2) and $^5D_0 \rightarrow {}^7F_1$ (I_1) transitions can be used to evaluate the local crystal field environment of the Eu^{3+} ion surroundings, and provide some information on the symmetry of the Eu^{3+} sites in the host lattice. The calculated R values are shown in the inset image in Fig. 5(a) as a function of the Bi^{3+} concentration. It can be seen that R increases with the Bi^{3+} concentration, and the highest R value of up to 3.48 was obtained for $KNEB_xN$ (x = 0.025), suggesting that the symmetry of the local crystal field of the Eu^{3+} ions decreased after adding Bi^{3+}, and the red light-emission from the $^5D_0 \rightarrow {}^7F_2$ transition is more closer to the optimal color chromaticity. These results are in agreement with the results of the structural analysis (Fig. 2).

To investigate the effect of the Bi^{3+} doping concentration on the emission intensity of the $KNEB_xN$ samples, the dependence of the red light-emission intensity of the $^5D_0 \rightarrow {}^7F_1$ transition

under 465 nm excitation on the Bi^{3+} concentration is shown in Fig. 5(b). Samples prepared with 5 mol% Bi_2O_3 addition show the strongest red light-emission, with an increase of almost 470% compared to the samples without Bi^{3+} doping. For samples prepared with a lower molar ratio of Bi_2O_3, the emission intensity monotonically increases with the Bi^{3+} concentration, whereas it greatly decreases for higher concentrations (> 5 mol% Bi_2O_3).

Several studies have shown that the emission peak (~ 485 nm) and the excitation peak (~ 380 nm) observed for Bi^{3+} ions correspond to the $^3P_1 \rightarrow {}^1S_0$ and the $^1S_0 \rightarrow {}^1P_1$ transition, respectively.[21,35] Combined with the results shown in Fig. 4, we found that, in the present study, the emission band of Bi^{3+} corresponding to the $^3P_1 \rightarrow {}^1S_0$ transition overlaps with the excitation bands of the Eu^{3+} ions, e.g., the $^7F_0 \rightarrow {}^5L_6$ (394 nm) and the $^7F_0 \rightarrow {}^5D_2$ (465 nm) transition. Therefore, we believe that the significant enhancement of the red light-emission with increasing Bi^{3+} concentration can mainly be ascribed to the effective energy transfer from Bi^{3+} to Eu^{3+}.

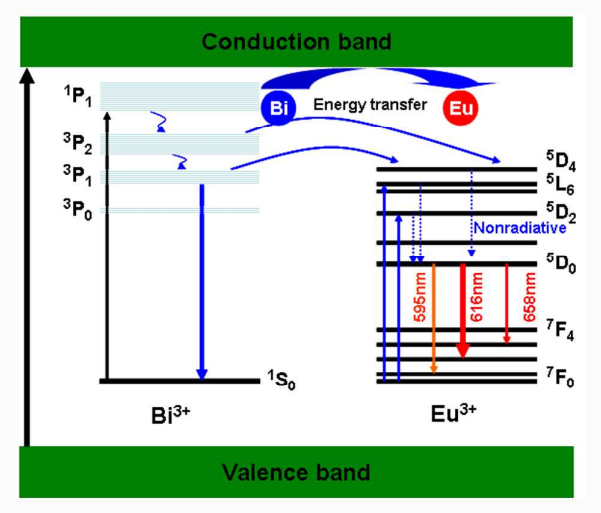

Fig. 6 The energy level and energy transfer diagram from Bi^{3+} to Eu^{3+} ions

The energy transfer mechanism between Bi^{3+} and Eu^{3+} ions can be described utilizing the energy level diagram, as shown in Fig. 6. For reasons of simplicity, only related energy states and

transitions are shown. When Bi^{3+} ions are excited to high level states, the energy absorbed by Bi^{3+} can be transferred to the $^5D_4$ level of the Eu^{3+} ions. At the same time, electrons on the $^7F_0$ ground state of Eu^{3+} are excited to the higher $^5L_6$ and $^5D_2$ levels, and radiationless de-excited to $^5D_0$ states. Subsequently, they recombine to ^7F_J (J=1,2) lower levels. Finally, the strong red light-emission at 616 nm was observed from the $^5D_0 \rightarrow {}^7F_2$ transition. The energy transfer process from Bi^{3+} to Eu^{3+} obviously depends on the Bi^{3+} doping concentration, as demonstrated by Fig. 5. When the Bi^{3+} concentration is higher than 0.05 mol, i.e., at a Bi^{3+} (sensitizer)/Eu^{3+} (activator) ratio higher than 1, more Bi^{3+} ions tend to form aggregates, as observed in other Bi^{3+}-doped materials.[36,37] These aggregates act as trapping centers and non-radiatively dissipate the absorbed energy, instead of transferring it to Eu^{3+}, thus leading to a decrease of the emission intensity of the Eu^{3+} ions.

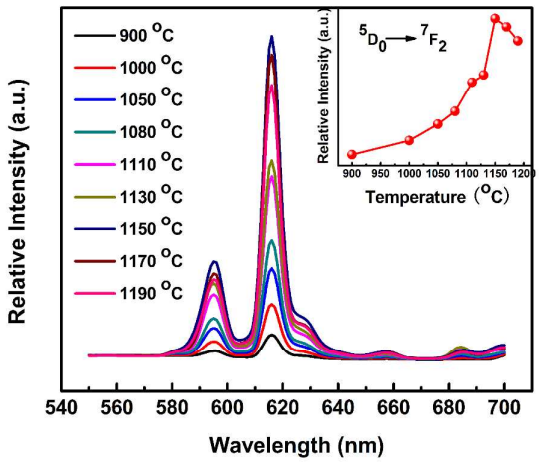

Fig. 7 PL spectra of the $KNEB_xN$ (x=0.05) sample with different sintering temperature excited by 465 nm at room temperature, the inset is the dependence of emission intensity ($^5D_0 \rightarrow {}^7F_2$) on sintering temperature.

In addition to the influence of the Bi^{3+} doping concentration, the sintering temperature must be taken into account as another important factor affecting the grain size, crystal size or crystal nature.

KNN-based ceramics are mostly fabricated within a narrow processing window in terms of the sintering temperature.[5,38,39] Therefore, it is necessary to find the optimal sintering temperature. The PL spectra of $KNEB_xN$ (x = 0.05) samples fabricated at different sintering temperatures recorded under excitation at 465 nm are shown in Fig. 7. In Fig. 7, the emission spectra show patterns similar to the patterns in Fig. 5, including two narrow band emissions attributed to transitions of the Eu^{3+} ions, i.e., $^5D_0 \rightarrow {}^7F_2$ (616 nm) and $^5D_0 \rightarrow {}^7F_1$ (593 nm). The strongest emission peak is still centered at 616 nm without a visible shift.

The influence of the sintering temperature on the emission intensity of the $^5D_0 \rightarrow {}^7F_2$ transition is shown in the inset image in Fig. 7. The PL emission intensity sharply increases as the sintering temperature increases from 900 °C to 1150 °C. The intensity decreases once the temperature exceeds 1150 °C. Generally, during the sintering process, the increase of the nucleation rate and enhanced crystallite growth with increasing temperature are very helpful for enhancing the emission intensity.[40] In the present study, some results, including the increased density of the microstructure, the increased grain size and the higher R values with increasing temperature, indicate an increased degree of crystallinity. As a result, the samples prepared at low sintering temperatures (below 1150 °C) show low PL intensities due to their low degree of crystallinity. Nevertheless, at a sintering temperature of up to 1150 °C, which is close to the melting point at 1200 °C, a high loss of Na, K or Bi and a consequential compositional deviation from the intended stoichiometry (K/Na=1) are unavoidable, as illustrated in Fig. 3, which might be the cause for the decreased PL intensity. Therefore, the optimum temperature for fabricating high-performance $KNEB_xN$ (x=0.05) luminescent materials is 1150 °C.

Based on the results above, an optimized red light-emission intensity was obtained by properly

controlling the Eu^{3+} content and the sintering temperature. For the $KNEB_xN$ system, the best results were found for 0.05 mol of Bi^{3+} and a sintering temperature of 1150 °C. To quantitatively evaluate the red light-emission intensity of the optimized sample composition, the absolute PL quantum yield (QY) (defined as the ratio of emitted photons to absorbed photons) was determined at room temperature using a combined steady state & time resolved fluorescence spectrometer (FLS920), and the results are shown in Fig 8. The sample doped with 0.05 mol of Bi^{3+} and sintered at 1150 °C shows a relatively high QY value of 0.34, which is comparable or superior to the recently reported QY values of RE-doped ferroelectric materials or some phosphors, such as $CaTiO_3$:Pr, BZCT:Pr, KNN:Pr, $Y_2O_2S/Y_2O_3:Eu^{3+}$.[11,39,41-43]

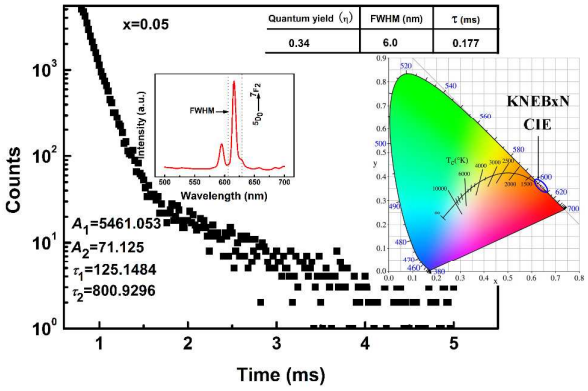

Fig. 8 The decay curve of the $KNEB_xN$ (x=0.05), and the insets are the quantum yield and CIE chromaticity diagram.

The chromaticity coordinates (CIE) of the $KNEB_xN$ (x = 0, 0.005, 0.015, 0.025, 0.04, 0.05, 0.07, 0.10, 0.15) samples for 465 nm excitation were calculated based on the emission spectra, and the results are shown on the inset image in Fig. 8 and compared in Table 1. The chromaticity coordinates only slightly change when the Eu^{3+} content is varied, indicating that adding Bi^{3+} does only slightly affect the emission color. The CIE chromaticity coordinates obtained for the $KNEB_xN$ (x = 0.05) sample are (x = 0.6476, y = 0.352), which is much closer to the National Television

Standard Committee (NTSC) coordinates for red color (x = 0.67, y = 0.33), and located in the red region.

In Fig. 8, we also measured the decay curve for the $^5D_0 \rightarrow {}^7F_2$ transition of the $KNEB_xN$ (x = 0.05) sample and determined the PL decay time, based on a double exponential fit, as follows:

$$I(t) = I_0 + A_1 \exp(-t/\tau_1) + A_2 \exp(-t/\tau_2) \quad (1)$$

where $I(t)$ and I_0 correspond to the emission intensity at time t and 0, respectively, A_J(J=1,2) is a constant, and τ_1 and τ_2 represent the decay times of the exponential components. The average decay lifetimes (t) can be obtained using the following equation:

(2)

The lifetimes calculated for the $^5D_0 \rightarrow {}^7F_2$ transition in the $KNEB_xN$ (x = 0.05) sample are τ_1 = 0.125 ms and τ_2 = 0.801 ms, respectively. Thus, the average lifetime (t) of the $^5D_0 \rightarrow {}^7F_2$ transition is about 0.177 ms. Compared to the average lifetime of the $^5D_0 \rightarrow {}^7F_1$ (593 nm) transition (t = 0.050 ms), the long lifetime of the $^5D_0 \rightarrow {}^7F_2$ transition would result in a high energy transfer efficiency, with strong red light-emission at 616 nm.

3.3. Thermal stability and water resistance behavior

For the practical application of high-power W-LEDs, the luminescent materials are required to withstand temperatures of up to 150 °C resulting from the very high excitation energy of LED chips.[44] Therefore, these materials need to exhibit a high thermal stability. Fig. 9 shows the temperature dependence of the PL emission intensity for the $KNEB_xN$ (x = 0.05) sample in the temperature range from room temperature to 320 °C. The temperature dependence of the integrated emission intensity normalized to the integral at 20 °C is shown in the inset imagine in Fig. 9. Under 465 nm excitation, the red-light emission intensity at 616 nm firstly increases and reaches its

maximum at 100 °C. At 150 °C, the intensity retained about 83% of the initial intensity at 20 °C. When the temperature was further increased to values above 160 °C, the emission intensity became dramatically quenched. In summary, the $KNEB_xN$ (x = 0.05) sample has a good thermal stability in the temperature range from 20 °C to 160 °C, and is therefore superior to the present commercial red phosphor, e.g. YAG:Ce^{3+}, SrS:Eu^{2+}, or Y_2O_3:Eu^{3+}.[40,45,46]

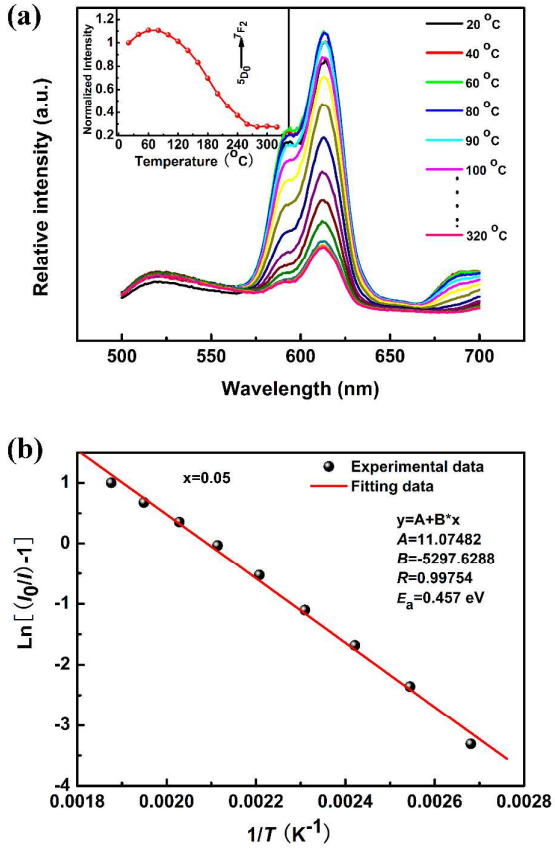

Fig. 9 (a) The normalized PL intensity of the $^5D_0 \rightarrow {}^7F_2$ transition as a function of temperature excited at 465 nm for $KNEB_xN$ (x=0.05). (b) The fitting curve of $Ln[(I_0/I_1)-1]$ vs. $1/T$ for $KNEB_xN$ (x=0.05).

The temperature dependence of the emission intensity was obtained using the Arrhenius equation:[47]

$$I(T) = \frac{I_0}{1 + c\exp(-E_a / kT)} \quad (3)$$

where I_0 and $I(T)$ are the emission intensity at the initial temperature and a second temperature T, c is a rate constant, E_a is the activation energy of the thermal-quenching process, and k is the Boltzmann constant (8.629×10^{-5} eV/K). The values of E_a were obtained from the slope of the fitting curves, i.e., $\ln[(I_0/I)-1]$ versus $1/kT$, as indicated in Fig. 8(b). The thermal-quenching activation energy E_a was calculated to approx. 0.457 eV.

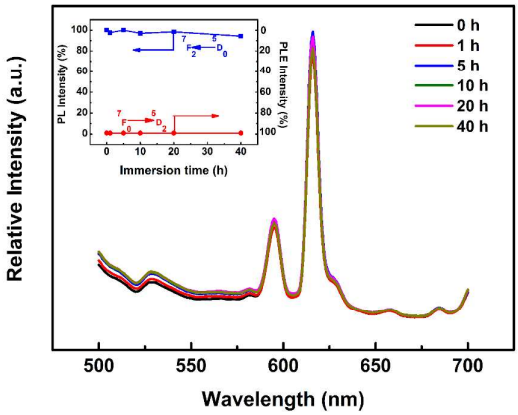

Fig. 10 PL spectra of $KNEB_xN$ (x=0.05) sample with various immersion time, the inset is immersion time (h) dependence of relative PL and PLE intensity from $^5D_0 \rightarrow {}^7F_2$ transition.

In some applications, the luminescent material or the entire device could be exposed to different environmental conditions, for example, an aqueous environment. It has been reported that the luminescence intensity of some alkali earth sulfide-, oxysulfide- and aluminate-based (e.g. $ZnS:Mn^{2+}$ or $SrAl_2O_4:Eu^{2+}$) red phosphors rapidly decreases after immersion in water due to hydrolysis reactions. As a result, the application potential of these materials is rather limited.[48,49] Thus, a material suitable for practical application not only needs to show a high luminescence

efficiency and thermal stability, but also a superior resistance to water. For this purpose, the water resistance behavior of the $KNEB_xN$ ($x = 0.05$) sample was investigated.

The PLE and PL spectra of the $KNEB_xN$ ($x = 0.05$) sample recorded for different immersion times (0 h, 1 h, 5 h, 10 h, 20 h and 40 h) are shown in Fig. 10. The emission spectra for an excitation at 616 nm and the excited intensity at 465 nm show only a very slight decrease in intensity with increasing immersion time (inset image in Fig. 10), retaining approx. 94.3% of the initial intensities after 40 h of immersion. These results indicate that KNN materials co-doped with Bi^{3+} and Eu^{3+} are suitable for an application in an aqueous environment due to their excellent resistance to water.

4. Conclusions

In summary, a novel red light-emitting material based on KNN co-doped with Bi^{3+} and Eu^{3+} was fabricated by the conventional solid state reaction method. The influence of the doping concentrations, the sintering temperature and the water immersion time on the photoluminescence properties were systematically investigated. The results showed that the PL spectra of the samples exhibited strong narrow red light-emissions at 616 nm, originating from the $^5D_0 \rightarrow {}^7F_2$ (616 nm) transition of Eu^{3+}, under excitation at 465 nm, which makes the material compatible with all commercial blue LED chips. The emission intensity and quantum yield can be effectively enhanced by adding Bi^{3+} ions (as sensitizer) as an alternative to increasing the Eu^{3+} concentration, and reach a maximum at a Bi^{3+} doping content of 0.05 mol. The optimal composition with $x = 0.05$ resulted in a high quantum yield of $\eta = 0.34$, a good thermal stability and superior water resistance properties. These experimental results indicate that the novel red light-emitting material based on a $(K_{0.5}Na_{0.5})NbO_3$ matrix co-doped with Bi^{3+} and Eu^{3+} ions, combined with its already admirable intrinsic piezoelectric properties, is a promising candidate for a future application in novel

multifunctional devices.

Acknowledgments

This work was supported by the Natural Science Foundation of China (No. 51462028 and 51072136), the Natural Science Foundation of Inner Mongolia (No. 2014MS0522 and 2014BS0202) and the Innovation Fund Project of Inner Mongolia University of Science and Technology (No. 2012NCL006 and 2012NCL002)

References

[1] W.F. Liu and X.B. Ren , Phys. Rev. Lett., 2009, 103, 257602.

[2] Z.H. Luo, J. Glaum, T. Grranzow, W. Jo, R. Dittmer, M. Hoffman and J. Rödel, J. Am. Ceram. Soc., 2011, 94(2), 529.

[3] Y. Saito, H. Takao, T. Tani, T. Nonoyama, K. Takatori, T. Homma, T. Nagaya and M. Nakamura, Nature, 2004, 432, 84.

[4] K. Uchino, Piezoelectric Actuators and Ultrasonic Motors. Kluwer Academic Publishers, Boston, 1997.

[5] J.F. Li, K. Wang, F.Y Zhu, L.Q. Cheng and F.Z. Yao, J. Am. Ceram. Soc., 2013, 96(12), 3677.

[6] Y.S. Sung, S. Baik, J.H. Lee, G.H. Ryu, D. Do, T.K. Song, M.H. Kim and W.J. Kim, Appl. Phys. Lett., 2012, 101, 012902.

[7] R.Z. Zuo, J. Fu and D.Y. Lv, J. Am. Ceram. Soc., 2009, 92[1], 283.

[8] S. Pin, F. Piccinelli, K.U. Kumar, S. Enzo, P. Ghigna, C. Cannas, A. Musinu, G. Mariotto, M. Bettinelli and A. Speghini, J. Solid State Chem., 2012, 196, 1.

[9] X. Wu, K.W. Kwok and F.L. Li, J. Alloys. Comp., 2013, 580, 88.

[10] R.S. Chaliha, K.Annapurna, A. Tarafder, V.S. Tiwari, P.K. Gupta and B. Karmakar, Opt. Mater., 2010, 32, 1202.

[11] H.Q. Sun, D.F. Peng, X.S. Wang, M.M. Tang, Q.W. Zhang and X. Yao, J. Appl. Phys., 2012, 111, 046102.

[12] X. S. Wang, C. N. Xu, H. Yamada, K. Nishikubo and X. G. Zheng, Adv. Mater., 2005, 17, 1254.

[13] H. Ryu, B. K. Singh, K. S. Bartwal, M. G. Brik and I. V. Kityk, Acta Materialia, 2008, 56,

358.

[14] J. H. Hao, Y. Zhang and X. H. Wei, Angew. Chem., 2011, 123, 7008.

[15] H.Q. Sun, D.F. Peng, X.S. Wang, M.M. Tang, Q.W. Zhang and X. Yao, J. Appl. Phys., 2011, 110, 016102.

[16] R. López-Juárez, R. Castañeda-Guzmán, F. Rubio-Marcos, M.E. Villafuerte-Castrejón, E. Barrera-Calva and F. González, Dalton Trans., 2013, 42, 6879.

[17] Y.B. Wei, Z. Wu, Y.M. Jia, J. Wu, Y.C. Shen and H.S. Luo, Appl. Phys. Lett., 2014, 105, 042902.

[18] Q.L. Dai, H.W. Song, M.Y. Wang, X. Bai, B. Dong, R.F. Qin, X.S. Qu and H. Zhang, J. Phys. Chem. C, 2008, 112(49), 19399.

[19] T.W. Kuo, W.R. Liu and T.M. Chen, Opt. Express, 2010, 18(8), 8187.

[20] N. Kimura, K. Sakuma, S. Hirafune, K. Asano, N. Hirosaki and R.J. Xie, Appl. Phys. Lett., 2007, 90, 051109.

[21] W.R. Liu, C.C. Lin, Y.C. Chiu, Y.T. Yeh, S.M. Jang, and R.S. Liu, Opt. Express, 18(3), 2946 (2010).

[22] P. Pust, V. Weiler, C. Hecht, A. Tücks, A.S. Wochnik, A.K. Henß, D. Wiechert, C. Scheu, P.J. Schmidt and W. Schnick, Nat. Mater., 2014, 13, 891.

[23] H.D. Xie, J. Lu, Y. Guan, Y.L. Huang, D.L. Wei and H.J. Seo, Inorg. Chem., 2014, 53(2), 827.

[24] S.K. Mahesh, P.P. Rao, M. Thomas, T.L. Francis and P. Koshy, Inorg. Chem., 2013, 52(23), 13304.

[25] L.L. Wang, Q.L. Wang, X.Y. Xu, J.Z. Li, L.B. Gao, W.K. Kang, J.S. Shi and J. Wang, J. Mater. Chem. C, 2013, 1, 8033.

[26] X. Min, Z.H. Huang, M.H. Fang, Y.G. Liu, C. Tang and X.W. Wu, Inorg. Chem., 2014, 53, 6060.

[27] R. K. Datta, J. Electrochem. Soc., 1967, 114(10), 1057.

[28] T.H. Fang, Y.J. Hsiao, Y.S. Chang and Y.H. Chang, Mater. Chem. Phys., 2006, 100, 418.

[29] A.F. Tian, W. Ren, L.Y. Wang, H.L. Du and X. Yao, Mater. Sci. Eng. B, 2013, 178, 1240.

[30] S.X. Yan, J.H. Zhang, X. Zhang, S.Z. Lu, X.G. Ren, Z.G. Nie and X.J. Wang, J. Phys. Chem., 2007, 111, 13256.

[31] J.F. Li, K. Wang, F.Y. Zhu, L.Q. Cheng and F.Z. Yao, J. Am. Ceram. Soc., 2013, 96(12), 3677.

[32] Y.H. Zhen and J.F. Li, J. Am. Ceram. Soc., 2006, 89(12), 3669.

[33] S. Nakamura and G. Fasol, The blue laser diode: GaN based light emitters and lasers (Springer,Berlin,1997).

[34] M.J. Weber, Phys. Rev., 1967, 157(2), 262.

[35] P. Boutinaud, Inorg. Chem., 2013, 52, 6028.

[36] H.N. Luitel, T. Watari, R. Chand, T. Torikai and M. Yada, Opt. Mater., 2012, 34, 1375.

[37] W.J. Park, M.K. Jung, S.J. Im and D.H. Yoon, Colloids and Surfaces A: Physicochem. Eng. Aspects, 2008, 313–314, 373.

[38] W.N. Wang, W. Widiyastuti, T. Ogi, I.W. Lenggoro and K. Okuyama, Chem. Mater., 2007, 19, 1723.

[39] Q.W. Zhang, H.Q. Sun, X.S. Wang, Y. Zhang and X. Li, J. Eur. Ceram. Soc., 2014, 34, 1439.

[40] X.Y. Yang, J. Liu, H. Yang, X.B. Yu, Y.Z. Guo, Y.Q. Zhou and J.Y. Liu, J. Mater. Chem., 2009, 19, 3771.

[41] P.T. Diallo, P. Boutinaud, R. Mahiou and J.C. Cousseins, Phys. Stat. Sol (A), 1997, 160, 255.

[42] D.F. Peng, H.Q. Sun, X.S. Wang, J.C. Zhang, M.M. Tang and X. Yao, Mater. Sci. Eng. B, 2011, 176, 1513.

[43] X.B. Qiao, Y. Cheng, L. Qin, C.X. Qin, P.Q. Cai, S.I. Kim and H.J. Seo, J. Alloys. Compd., 2014, 617, 946.

[44] C. Feldman, T. Jüstel, C.R. Ronda and P.J. Schmidt, Adv. Funct. Mater., 2003, 13, 51.

[45] T.W. Kuo, C.H. Huang and T.M. Chen, Opt. Express, 2010, 18(102), A231.

[46] Z. Sun, G.X. Cao, Q.H. Zhang, Y.G. Li and H.Z. Wang, Mater. Chem. Phys., 2012, 132, 937.

[47] S. Murakami, M. Herren, D. Rau and M. Morita, Inorg. Chim. Acta, 2000, 300-342, 1014.

[48] L. Zhang, H. Yamada, Y. Imai and C.N. Xu, J. Electrochem. Soc., 2008, 155, J63.

[49] Y. Imai, R. Momoda, Y. Adachi, K. Nishikubo, Y. Kaida, H. Yamada and C.N. Xu, J. Electrochem. Soc., 2007, 154, J77.

Table I. The photoluminescence properties and CIE chromaticity coordinates of KNN materials co-doped Bi^{3+} and Eu^{3+} ions

Samples	λ_{ex} (nm)	CIE chromaticity coordinate		QY (η)	$^5D_0 \rightarrow {}^7F_2$ Relative intensity
		x	**y**		
$(K_{0.5}Na_{0.5})_{0.95}Eu_{0.05}NbO_3$	465	0.6348,	0.3648	--	1.00
$(K_{0.5}Na_{0.5})_{0.945}Eu_{0.05}Bi_{0.005}NbO_3$	465	0.6345,	0.3651	--	1.43
$(K_{0.5}Na_{0.5})_{0.935}Eu_{0.05}Bi_{0.015}NbO_3$	465	0.6378,	0.3618	--	1.80
$(K_{0.5}Na_{0.5})_{0.925}Eu_{0.05}Bi_{0.025}NbO_3$	465	0.6463,	0.3534	--	3.31
$(K_{0.5}Na_{0.5})_{0.95-x}Eu_{0.05}Bi_{0.04}NbO_3$	465	0.6461,	0.3535	--	3.83
$(K_{0.5}Na_{0.5})_{0.95-x}Eu_{0.05}Bi_{0.05}NbO_3$	465	0.6476,	0.3520	0.34	4.77
$(K_{0.5}Na_{0.5})_{0.95-x}Eu_{0.05}Bi_{0.07}NbO_3$	465	0.6270,	0.3726	--	3.52
$(K_{0.5}Na_{0.5})_{0.95-x}Eu_{0.05}Bi_{0.10}NbO_3$	465	0.6429,	0.3567	--	3.10
$(K_{0.5}Na_{0.5})_{0.95-x}Eu_{0.05}Bi_{0.15}NbO_3$	465	0.6380,	0.3616	--	0.56
$Y_2O_3S:Eu^{3+}$[40]	394	--		0.35	--
$Y_2O_3:Eu^{3+}$[41]	465	--		<1%	--

Figures captions

Fig. 1 Schematic of the sintering process of the $KNEB_xN$ ceramics.

Fig. 2 (a) SEM image of the selected $KNEB_xN$ (x=0.05) sample. (b) The perovskite type ABO_3 subcell of KNN. (c) XRD patterns of $KNEB_xN$ ceramics (x=0, 0.005, 0.045, 0.025, 0.040, 0.050,0.070, 0.100, 0.150). (d) The diffraction peaks from 44.5^o to 47.5^o.

Fig. 3 The degree of volatilization of K, Na and Bi elements in $KNEB_xN$ ceramics (x=0.005, 0.050, 0.150), the inset is K/Na mole ration as a function of Bi concentrations.

Fig. 4 Room temperature PLE, PL and diffuse reflectance spectra of the $KNEB_xN$ (x=0.05) sample.

Fig. 5 (a) PL spectra of the $KNEB_xN$ ceramics (x=0, 0.005, 0.045, 0.025, 0.040, 0.050,0.070, 0.100, 0.150) excited by 465 nm at room temperature, the inset is the intensity ratio of I_2/I_1 on Bi^{3+} concentrations. (b) The dependence of the emission intensity ($^5D_0 \rightarrow {}^7F_2$) on Bi^{3+} concentrations.

Fig. 6 The energy level and energy transfer diagram from Bi^{3+} to Eu^{3+} ions

Fig. 7 PL spectra of the $KNEB_xN$ (x=0.05) sample with different sintering temperature excited by 465 nm at room temperature, the inset is the dependence of emission intensity ($^5D_0 \rightarrow {}^7F_2$) on sintering temperature.

Fig. 8 The decay curve of the $KNEB_xN$ (x=0.05), and the insets are the quantum yield and CIE chromaticity diagram.

Fig. 9 (a) The normalized PL intensity of the $^5D_0 \rightarrow {}^7F_2$ transition as a function of temperature excited at 465 nm for $KNEB_xN$ (x=0.05). (b) The fitting curve of $Ln[(I_0/I_1)-1]$ vs. $1/T$ for $KNEB_xN$ (x=0.05).

Fig. 10 PL spectra of $KNEB_xN$ (x=0.05) sample with various immersion time, the inset is immersion time (h) dependence of relative PL and PLE intensity from $^5D_0 \rightarrow {}^7F_2$ transition.